Wang *et al. Microstructures* 2023;3:2023023
DOI: 10.20517/microstructures.2023.04

Microstructures

Research Article

Open Access

Check for updates

High energy storage properties of $0.94Bi_{0.5}Na_{0.5}TiO_3$-$0.06BaTiO_3$ ceramics by incorporating $Sr_{0.8}Bi_{0.1}\square_{0.1}Ti_{0.8}Zr_{0.2}O_{2.95}$

Cheng Wang[1], Xiaojie Lou[2]

[1]Gansu Vocational College of Architecture, Lanzhou 730050, Gansu, China.
[2]Frontier Institute of Science and Technology, and State Key Laboratory for Mechanical Behavior of Materials, Xi'an Jiaotong University, Xi'an 710049, Shaanxi, China.

Correspondence to: Prof. Xiaojie Lou, Frontier Institute of Science and Technology, and State Key Laboratory for Mechanical Behavior of Materials, Xi'an Jiaotong University, No. 1 West Building, 99 Yanxiang Road, Yanta District, Xi'an 710049, Shaanxi, China. E-mail: xlou03@163.com

How to cite this article: Wang C, Lou X. High energy storage properties of $0.94Bi_{0.5}Na_{0.5}TiO_3$-$0.06BaTiO_3$ ceramics by incorporating $Sr_{0.8}Bi_{0.1}\square_{0.1}Ti_{0.8}Zr_{0.2}O_{2.95}$. *Microstructures* 2023;3:2023023. https://dx.doi.org/10.20517/microstructures.2023.04

Received: 16 Jan 2023 **First Decision:** 17 Feb 2023 **Revised:** 22 Mar 2023 **Accepted:** 5 May 2023 **Published:** 19 May 2023

Academic Editor: Shujun Zhang **Copy Editor:** Fangling Lan **Production Editor:** Fangling Lan

Abstract

Ceramics with high-energy storage density are in high demand across various industries. In this regard, lead-free relaxor ferroelectric ceramics were synthesized using the conventional solid-state reaction method with the composition $(1-x)[0.94Bi_{0.5}Na_{0.5}TiO_3-0.06BaTiO_3]-xSr_{0.8}Bi\gamma_{0.1}Ti_{0.8}Zr_{0.2}O_{0.95}$, abbreviated as BNBT-*x*SBTZ. The incorporation of SBTZ in BNBT ceramics significantly improved their relaxation properties. Specifically, the 0.91BNBT-0.09SBTZ ceramics displayed a breakdown electric field of up to 230 kV/cm, with a recoverable energy storage density (*Wr*) of 2.68 J/cm^3 and an energy storage efficiency (η) of 74.4%. Additionally, this sample demonstrated remarkable temperature stability and fatigue resistance, with only an 11% decrease in *Wr* observed from room temperature to 140 °C and a 13.3% reduction in *Wr* after 10^5 electrical cycles. Therefore, the 0.91BNBT-0.09SBTZ ceramic is a promising dielectric material suitable for energy-storage dielectric capacitors.

Keywords: Energy storage properties, lead-free ceramics, temperature stability, fatigue resistance

INTRODUCTION

The global community is facing the challenge of climate change and environmental issues, which

© The Author(s) 2023. **Open Access** This article is licensed under a Creative Commons Attribution 4.0 International License (https://creativecommons.org/licenses/by/4.0/), which permits unrestricted use, sharing, adaptation, distribution and reproduction in any medium or format, for any purpose, even commercially, as long as you give appropriate credit to the original author(s) and the source, provide a link to the Creative Commons license, and indicate if changes were made.

necessitates the exploration of alternative energy sources such as solar and wind power. However, the intermittent nature of these energy sources presents limitations on their practical applications. Therefore, it is crucial to develop new energy storage technologies. Currently, the primary electrical energy storage devices include batteries, chemical capacitors, and ceramic capacitors. Ceramic capacitors, in particular, offer many advantages, such as high-power density, rapid charging and discharging rates, and a broad operating temperature range. As a result, they are widely used in various applications, including pulsed power supplies, microwave circuits, and electric vehicles. Nevertheless, the low energy storage density of ceramic capacitors compared to chemical batteries restricts their potential applications. Consequently, there is an urgent need to develop ceramic capacitors with higher energy storage density to address the growing energy challenges.

The key performance indicators of ceramic capacitors comprise the recoverable energy storage density (W_r), total energy storage density (W), and energy storage efficiency (η). These parameters can be derived from the electrical hysteresis loops (P-E) of ceramics or calculated by following Equation (1-3)[1,2]:

$$W = \int_0^{P_m} EdP \tag{1}$$

$$W_r = \int_{P_r}^{P_m} EdP \tag{2}$$

$$\eta = \frac{W_r}{W} \tag{3}$$

where P_m is the maximum polarization, and P_r is the remanent polarization.

Equations (1-3) indicate that achieving high energy storage capacity (W_r) and efficiency (η) requires a large polarization (P_m) and a small remnant polarization (P_r). The ferroelectric ceramic $Na_{0.5}Bi_{0.5}TiO_3$ (BNT) possesses a large P_m, making it a promising candidate for developing high-energy storage capacitors. However, pristine BNT ceramic has a large P_r, resulting in low W_r and η. Recent studies have focused on developing BNT-based ceramics with large P_m and small P_r through doping, which can significantly reduce the grain size of the ceramics and increase their dielectric breakdown strength (DBS), W_r, and η[3]. For instance, Qi *et al.* prepared linear-like anti-ferroelectric BNT-based ceramics with a W_r of 7.02 J/cm^3 and η of 85%[4]. Similar results have been reported in other studies[5-8]. Therefore, chemical doping of pure BNT is an important method for preparing ceramics with high-energy storage properties.

The material $0.94Na_{0.5}Bi_{0.5}TiO_3$-$0.06BaTiO_3$ (BNT-BT) is a type of relaxor ferroelectric material that exhibits a morphotropic phase boundary (MPB) structure. When an external electric field is applied, this material undergoes a reversible transition from a relaxor state to a long-range ferroelectric order, resulting in a large P_m and a lower P_r[9,10]. However, the dielectric breakdown electric field of BNT-BT is relatively low. In general, the breakdown electric field of dielectric ceramics increases with decreasing grain size. Therefore, in this study, we aim to improve the breakdown electric field and enhance the energy storage properties of BNT-BT by using $Sr_{0.8}Bi_{0.1}\gamma_{0.1}Ti_{0.8}Zr_{0.2}O_{2.95}$ (SBTZ) as a modifier to regulate the relaxation behavior and decrease the grain size. SBTZ is a newly developed relaxor ferroelectric material obtained by doping Bi^{3+} and Zr^{4+} into the cubic-phase perovskite material of $SrTiO_3$. The introduction of Bi^{3+} and Zr^{4+} ions into the A-site of $SrTiO_3$ reduces the chemical ratio of Bi^{3+} and creates an A-site vacancy, which disrupts the ferroelectric order and results in relaxation behavior[11,12]. It is expected that the energy storage performance of BNT-BT

will be improved due to the enhanced relaxation property and breakdown electric field.

MATERIALS AND METHODS

Ceramic samples of (1-*x*)[0.94$Bi_{0.5}Na_{0.5}TiO_3$-0.06$BaTiO_3$]-*x*$Sr_{0.8}Biγ_{0.1}Ti_{0.8}Zr_{0.2}O_{0.95}$ (abbreviated as: (1-*x*)BNBT-*x*SBTZ, *x* = 0.07, 0.08, 0.09, and 0.10) were synthesized using the solid-state reaction method. The starting materials used were Bi_2O_3 (99.9%), Na_2CO_3 (99.5%), $BaCO_3$ (99.9%), $SrCO_3$ (99%), TiO_2 (99.6%), and ZrO_2 (99.99%). The raw powders were mixed and ball-milled for 16 h in polyethylene pots with zirconia balls and ethanol as the milling medium. The use of ethanol was preferred due to its low ion dissolution properties, which minimized the introduction of unwanted ions. The milled powder was dried, sieved, and formed into cylindrical pellets before being sintered for 4 h at 850 °C The sintered pellets were then crushed, re-milled for 10 h, and cold isostatically pressed into pellets with a diameter of 10 mm under a pressure of 250 MPa. The pellets were sintered at 1150 °C for 2 h in alumina crucibles in an air atmosphere. To compensate for the loss of sodium oxides and bismuth, the pellets were buried in prepared powders of the same composition. Finally, the sintered pellets were polished to a final thickness of approximately 0.6 mm, and silver electrodes were coated on both surfaces and fired at 550 °C for 30 min for electrical testing.

The phase structure was determined through the use of X-ray diffractometry (XRD, Advanced), while the surface morphology was analyzed by means of scanning electron microscopy (SEM) (Carle Zeiss GeminiSEM 500, Germany). In addition, the dielectric properties were measured using a precision impedance analyzer (Agilent E4980A), while Raman spectra were obtained using a Raman spectrometer (Horiba Allmentation LabRam). Finally, the polarization hysteresis loops (*P-E*) were assessed via a standard ferroelectric analyzer (TF Analyzer 2000).

RESULTS AND DISCUSSION

The X-ray diffraction patterns of BNBT-*x*SBTZ ceramics were analyzed in the range of 20° to 75°, as shown in Figure 1A. The results indicate that each sample has a single perovskite structure, with no presence of any secondary phase. This suggests that SBTZ is fully incorporated into the lattice[13]. Furthermore, Figure 1B displays the expanded XRD patterns around the diffraction peak of (111), which reveals that the diffraction peaks shift towards higher diffraction angles as the SBTZ doping content increases. This shift indicates a reduction in the lattice constant[14,15]. Additionally, the absence of peak splitting at around 40° suggests that all samples possess a highly symmetrical pseudocubic structure[16].

The Raman spectra of (1-*x*)BNBT-*x*SBTZ ceramics were analyzed in the range of 100-1,000 cm^{-1}, as depicted in Figure 1C. The spectra were categorized into four regions, each representing distinct chemical bonding behavior[17]. The modes below 200 cm^{-1} were found to be associated with A-site atomic vibrations, while the high-frequency band between 200 and 380 cm^{-1} corresponded to the vibrations of BO bonds, including Zr^{2+}, Zr^{4+}, and Ti^{4+} ions. The modes near 550 cm^{-1} and 610 cm^{-1} were linked to Ti/Zr-O_6 vibrations, and it was observed that the two peak positions became separated, indicating an increased intensity of oxygen octahedron vibration and enhanced relaxation characteristics with increasing doping content[18]. The section with modes above 700 cm^{-1} was considered to be the superposition of various vibration modes.

The SEM images of (1-*x*)BNBT-*x*SBTZ ceramics, as depicted in Figure 2A-D, indicate that the ceramics have been effectively sintered with minimal surface pores. The grain size of the ceramics initially decreases and then increases with increasing dopant concentration. This phenomenon can be attributed to the appearance of low melting point regions in the ceramics after SBTZ doping. During the sintering and cooling process, these regions are more prone to nucleation and grain growth, resulting in a decrease in grain size. However, at higher doping concentrations, the liquid phase melting regions further increase,

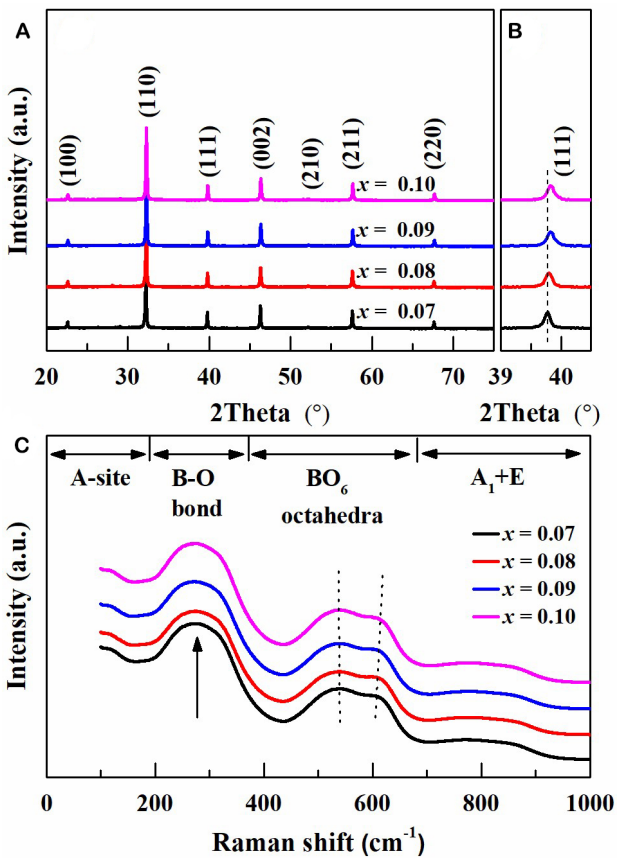

Figure 1. XRD patterns and Raman spectra of the sintered ceramics. (A) XRD patterns from 20° to 75°; (B) expanded XRD patterns at around peak (111); (C) Raman spectra in the range of 100-900 cm^{-1}.

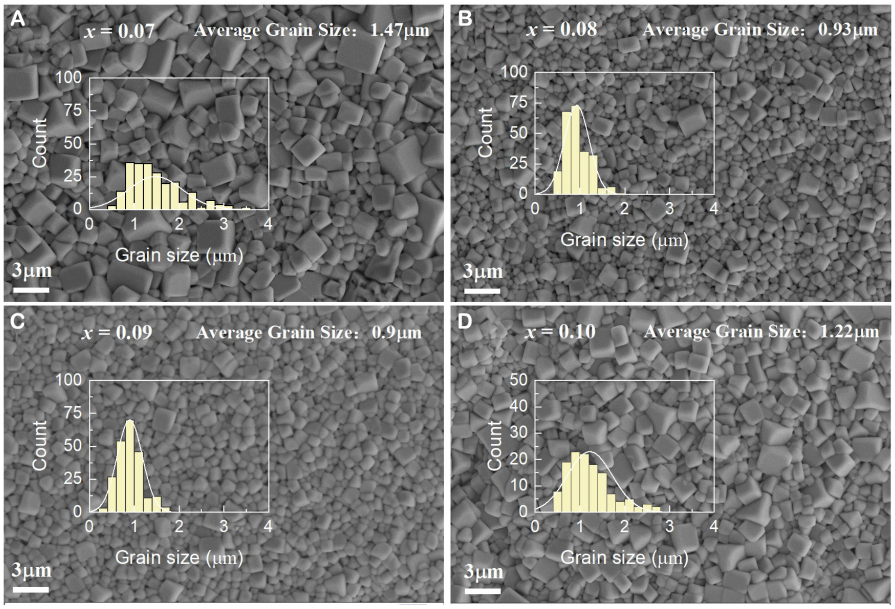

Figure 2. The surface morphology of the (1-*x*)BNBT-*x*SBTZ ceramics and distribution of grain size. (A) *x* = 0.07, (B) *x* = 0.09, (C) *x* = 0.09, and (D) *x* = 0.10.

leading to the emergence of smaller grain sizes[19]. The breakdown field of ceramics is significantly influenced by the grain size, with smaller grain sizes resulting in higher breakdown electric fields[18]. Therefore, the addition of SBTZ at low doping levels is advantageous for achieving high energy storage properties. Specifically, when the SBTZ content is 0.07, 0.08, 0.09, and 0.1, the average grain sizes are 1.47 μm, 0.93 μm, 0.90 μm, and 1.22 μm, respectively.

Figure 3 depicts the dielectric behavior of (1-x)BNBT-xSBTZ ceramics over a temperature range of 35-400 °C and at frequencies of 1 kHz, 10 kHz, 1 MHz, 10 MHz, and 20 MHz, respectively. The curves illustrate that the ceramics exhibit relaxation behavior with double dielectric peaks. The shape of the curves remains consistent across varying SBTZ doping levels, with the dielectric peak T_m becoming broader, indicating an enhanced relaxation characteristic[20]. The second peak T_m, which corresponds to the maximum dielectric constant (ε_m), represents the relaxation of the rhombohedral-tetragonal phase transition brought about by the polar nanoregions[21]. As the doping level increases, the ε_m of the ceramics tends to decrease, indicating a weakening of the ferroelectric properties. The low dielectric losses (tan δ) of the samples demonstrate their excellent insulating properties, which play a crucial role in improving the energy storage performance of ceramics.

In order to conduct a more thorough investigation into the relaxor transition in ceramics, an adaptation of the Curie-Weiss Law was implemented, which can be expressed as follows:

$$\ln(1/\varepsilon - 1/\varepsilon_{max}) = \gamma \ln(T - T_m) + C \quad (4)$$

where ε is the dielectric constant, T is the temperature, T_m is the temperature at which ε reaches its maximum value ε_{max}, C is a constant, and is the diffuse degree. The value of γ ranges from 1 for typical ferroelectrics to 2 for ideal relaxor ferroelectrics.

Figure 4 depicts the relationship between $\ln(T-T_m)$ and $\ln(1/\varepsilon - 1/\varepsilon_{max})$ for the examined samples. The calculated value of γ ranges from 1.76 to 2.01, indicating a strong relaxation behavior of the sintered ceramics.

The dielectric breakdown strength (DBS) of the ceramics was evaluated, as depicted in Figure 5A. By utilizing the Weibull distribution as Equation (5-7)[22]:

$$P_i = i/(n+1) \quad (5)$$

$$X_i = \ln(E_i) \quad (6)$$

$$Y_i = \ln(\ln(1/(1-P_i))) \quad (7)$$

where i is the group number, X_i and Y_i are parameters in Weibull distribution functions, E_i is the DBS of sample i, P_i is associated with dielectric breakdown, and n is the sum of specimens of each sample. The electric field is ranged as Equation (8).

$$E_1 \le E_2 \le \ldots \le E_i \le \ldots \le E_n \quad (8)$$

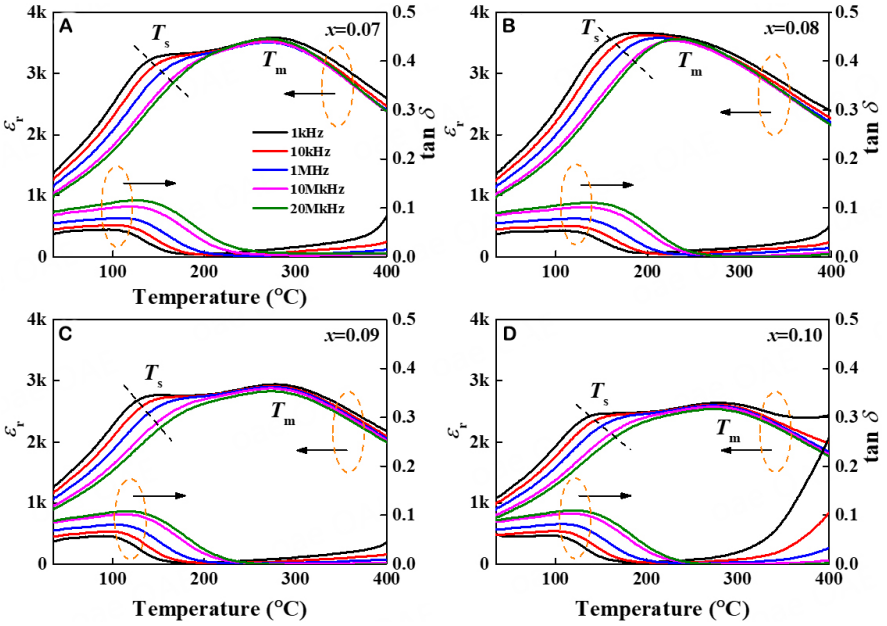

Figure 3. Temperature-dependent dielectric permittivity and loss of (1-*x*)BNBT-*x*SBTZ ceramics from 70 to 400 °C at 1 kHz, 10 kHz, 1 MHz, 10 MHz, and 20 MHz, respectively. (A) *x* = 0.07, (B) *x* = 0.09, (C) *x* = 0.09, and (D) *x* = 0.10.

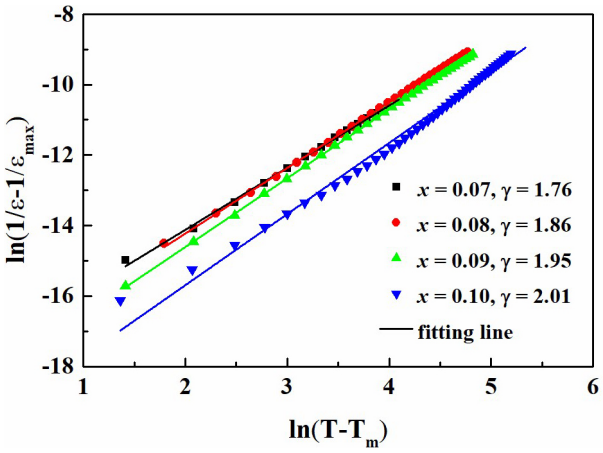

Figure 4. Plots of $\ln(1/\varepsilon\text{-}1/\varepsilon_{max})$ as a function of $\ln(T\text{-}T_m)$ at 1 kHz by the modified Curie-Weiss law.

According to the Weibull distribution model, there is a linear relationship between X_i and Y_i, as shown in Equation (9).

$$Y_i = mX_i + b \tag{9}$$

where m represents the dispersion degree of all experimental data, and a larger m indicates more reliable experimental results.

The determination of the magnitude of DBS can be derived from the intercept on the $\ln(E_i)$ axis. The results obtained from the fitted calculations in Figure 5A indicate that the DBS gradually increases and then

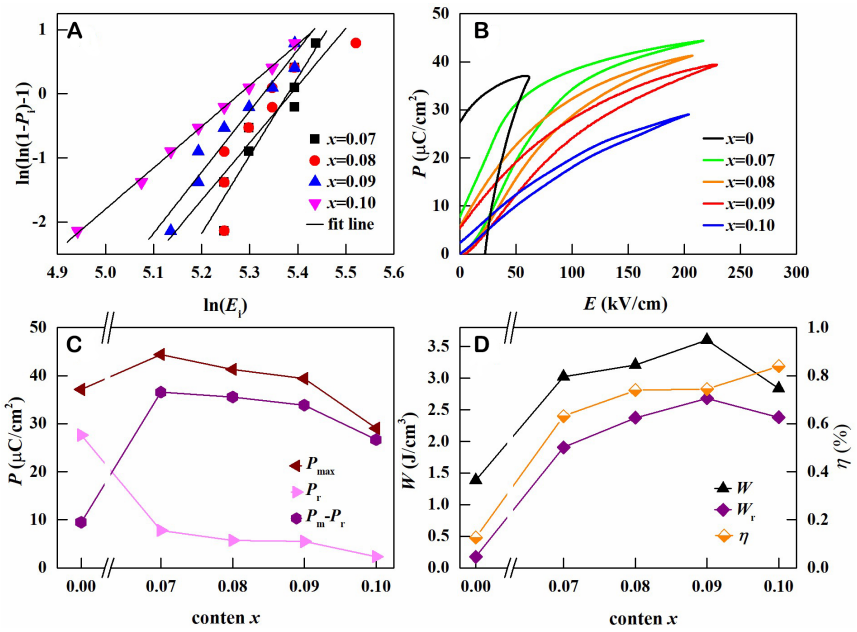

Figure 5. Energy storage studies of sintered (1-*x*)BNBT-*x*SBTZ ceramics. (A) Weibull distribution of the breakdown electric field; (B) *P-E* loops as a function of *x*; (C) P_m, P_r, and P_m-P_r as a function of *x*; (D) W_r, W, and η as a function of *x*.

decreases with the increase of SBTZ content, which is consistent with the shift in the average grain size. The DBS values obtained for increasing dopant concentrations were 215 kV/cm, 230 kV/cm, 245 kV/cm, and 218 kV/cm, respectively. The DBS is influenced by several factors, including porosity, grain size, and extrinsic measurement conditions such as sample thickness, sample area, and electrode configuration. In this study, all the samples had almost the same phase structure and measurement condition, but there was a slight difference in grain size. Generally, smaller grain size contributes to an enhanced DBS, and furthermore, the DBS exhibits an opposite variation tendency with grain size[23-25].

The polarization hysteresis (*P-E*) loops of the sintered BNBT-xSBTZ ceramics were measured and shown in Figure 5B. The test electric field was loaded near the breakdown field. The *P-E* loops were observed to be flat and slender, indicating weak ferroelectricity and enhanced relaxation properties. This is a crucial factor in achieving high energy storage density and efficiency[26]. As the doping content increased, P_{max}, P_r, and P_{max}-P_r gradually decreased, as depicted in Figure 5C. The trend of decreasing polarization intensity also suggests a decline in ferroelectricity. The sample with 0.93BNBT-0.07SBTZ exhibited the highest P_{max} of 44.38 μC/cm², but its W_r was not the highest due to its high P_r. In contrast, the 0.9BNBT-0.1SBTZ sample had a lower P_{max} of 29.04 μC/cm² and P_r of 2.36 μC/cm². Figure 5D illustrates the values of W, W_r, and η for all samples. It was observed that W_r reached its maximum value at x=0.09, while η was highest at x=0.10. The values of W, W_r, and η are presented in Table 1.

The practical application of energy storage ceramics requires good temperature stability. To investigate the temperature stability of the 0.91BNBT-0.09SBTZ ceramic, energy storage characteristics were examined at various temperatures. *P-E* hysteresis loops were measured at 170 kV/cm, with temperatures ranging from 25 °C to 140 °C, as depicted in Figure 6A. The *P-E* loops did not exhibit significant changes, with P_{max} decreasing from 34.7 μC/cm² at 25 °C to 31.6 μC/cm² at 140 °C. Additionally, W_r decreased from 1.71 J/cm³ to 1.52 J/cm³, as shown in Figure 6B. Despite the temperature variations, W_r and η remained at a relatively high level, indicating excellent temperature stability.

Table 1. Energy storage properties of (1-*x*)BNBT-*x*SBTZ ceramics

x	*W* (J/cm^3)	W_r (J/cm^3)	*E* (kV/cm)	η
0	1.38	0.174	60	12.6%
0.07	3.02	1.91	215	63.1%
0.08	3.21	2.37	230	73.9%
0.09	3.60	2.68	245	74.4%
0.10	2.84	2.38	218	83.9%

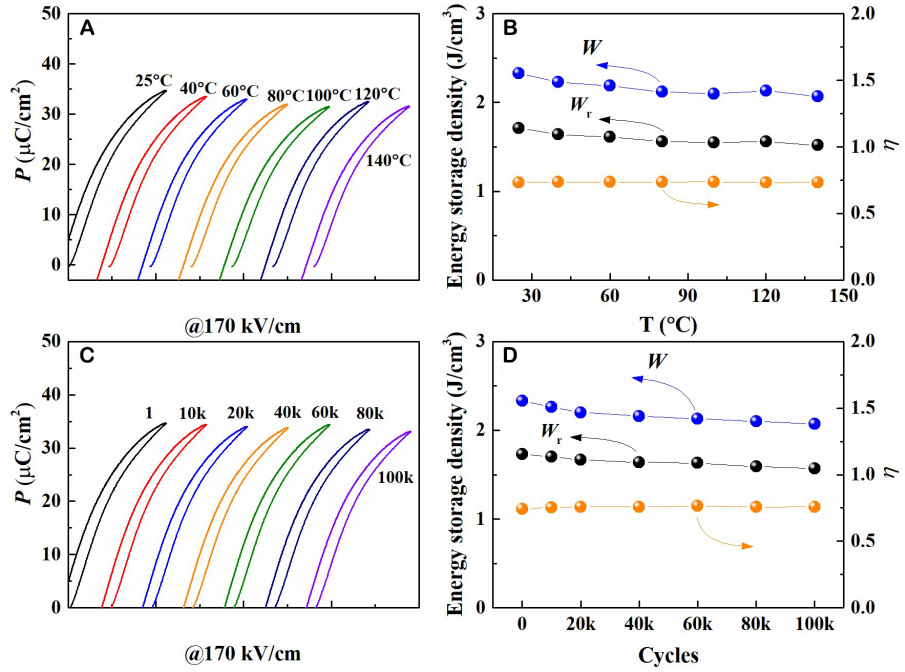

Figure 6. Temperature stability and fatigue resistance of the sintered ceramics. (A) *P-E* hysteresis loops at 25 °C to 140 °C; (B) W_r and η as a function of temperature; (C) fatigue behavior measured at various electrical cycles; (D) W_r and η as a function of electrical cycles.

In addition to examining the temperature stability of ceramics, their fatigue resistance behavior was also investigated. The fatigue behavior was assessed at room temperature under a frequency of 10 Hz and a voltage of 170 kV/cm, with a cycling number of 10^5. The *P-E* loops at different cycles were depicted in Figure 6C, while the changes in P_{max} and W_r with an increase in the number of charging/discharging cycles were illustrated in Figure 6D. After 10^5 cycles, W_r remained at a relatively high level of 1.5 J/cm^3, which was only 13.3% lower than its initial value of 1.73 J/cm^3, indicating favorable fatigue resistance properties. It is worth noting that P_{max} and W_r exhibited a slight decrease, which was attributed to the local phase decomposition caused by switching-induced charge injection, as suggested by Lou *et al.*[27-29].

CONCLUSIONS

This study investigated the dielectric and energy storage properties of (1-*x*)(0.94$Bi_{0.5}Na_{0.5}TiO_3$-0.06$BaTiO_3$) -*x*$Sr_{0.8}Bi_{0.1}\gamma_{0.1}Ti_{0.8}Zr_{0.2}O_{2.95}$ ceramics, prepared through the solid-state method. X-ray diffraction analysis revealed a single perovskite structure in all ceramic samples, indicating successful incorporation of SBTZ into the BNBT lattice. Doping with SBTZ resulted in notable relaxation properties and excellent energy storage capabilities. Specifically, 0.91BNBT-0.09SBTZ ceramics demonstrated a breakdown electric field of 230 kV/cm, with W_r of 2.68 J/cm^3 and η of 74.4%. Additionally, the energy storage properties of the ceramics

exhibited remarkable temperature stability and fatigue resistance. The energy storage density only decreased by 11% from room temperature to 140 °C, and after 10^5 electrical cycles, the energy storage density decreased by only 5.2%. Overall, these findings suggest that 0.91BNBT-0.09SBTZ ceramics have great potential as dielectric materials for energy-storage dielectric capacitors.

DECLARATIONS

Authors' contributions

Made substantial contributions to the conception and design of the study and performed data analysis and interpretation: Wang C

Performed data acquisition and provided administrative, technical, and material support: Lou X

Availability of data and materials

Not applicable.

Financial support and sponsorship

This work was supported by the Education Science and Technology Innovation Project of Gansu Province, China, the year of 2022; the project: Study on the mechanism of the fatigue behavior of sodium-bismuth-titanate based relaxor ferroelectric capacitors after electrical charge-discharge cycles (Grant No. 2022QB-213) and the National Natural Science Foundation of China (NSFC NO.52172125).

Financial support and sponsorship

None.

Conflicts of interest

Both authors declared that there are no conflicts of interest.

Ethical approval and consent to participate

Not applicable.

Consent for publication

Not applicable.

Copyright

© The Author(s) 2023.

REFERENCES

1. Yang L, Kong X, Li F, et al. Perovskite lead-free dielectrics for energy storage applications. *Prog Mater Sci* 2019;102:72-108. DOI
2. Zou K, Dan Y, Xu H, et al. Recent advances in lead-free dielectric materials for energy storage. *Mater Res Bull* 2019;113:190-201. DOI
3. Shi P, Li T, Zhu X, et al. High strain in $Bi_{0.5}Na_{0.5}TiO_3$-based relaxors by adding two modifiers featuring with morphotropic phase boundary. *Scripta Mater* 2022;218:114674. DOI
4. Qi H, Zuo R. Linear-like lead-free relaxor antiferroelectric $(Bi_{0.5}Na_{0.5})TiO_3$-$NaNbO_3$ with giant energy-storage density/efficiency and super stability against temperature and frequency. *J Mate Chem A* 2019;8:3971-8. DOI
5. Zhu X, Shi P, Gao Y, et al. Enhanced energy storage performance of $0.88(0.65Bi_{0.5}Na_{0.5}TiO_3$-$0.35SrTiO_3)$-$0.12Bi(Mg_{0.5}Hf_{0.5})O_3$ lead-free relaxor ceramic by composition design strategy. *Chem Eng J* 2022;437:135462. DOI
6. Lv J, Li Q, Li Y, et al. Significantly improved energy storage performance of NBT-BT based ceramics through domain control and preparation optimization. *Chem Eng J* 2021;420:129900. DOI
7. Luo C, Feng Q, Luo N, et al. Effect of Ca^{2+}/Hf^{4+} modification at A/B sites on energy-storage density of $Bi_{0.47}Na_{0.47}Ba_{0.06}TiO_3$ ceramics. *Chem Eng J* 2021;420:129861. DOI
8. Yao Y, Li Y, Sun N, et al. Enhanced dielectric and energy-storage properties in ZnO-doped $0.9(0.94Na_{0.5}Bi_{0.5}TiO_3$-$0.06BaTiO_3)$-$0.1NaNbO_3$ ceramics. *Ceram Int* 2018;44:5961-6. DOI

9. Ma C, Tan X, Dul'kin E, Roth M. Domain structure-dielectric property relationship in lead-free (1-*x*)($Bi_{1/2}Na_{1/2}$)TiO_3-*x*$BaTiO_3$ ceramics. *J Appl Phys* 2010;108:104105. DOI
10. Ma C, Guo H, Beckman SP, Tan X. Creation and destruction of morphotropic phase boundaries through electrical poling: a case study of lead-free ($Bi_{1/2}Na_{1/2}$)TiO_3-$BaTiO_3$ piezoelectrics. *Phys Rev Lett* 2012;109:107602. DOI
11. Li T, Lou X, Ke X, et al. Giant strain with low hysteresis in a-site-deficient ($Bi_{0.5}Na_{0.5}$)TiO_3-based lead-free piezoceramics. *Acta Mater* 2017;128:337-44. DOI
12. Cao W, Li W, Feng Y, et al. Defect dipole induced large recoverable strain and high energy-storage density in lead-free $Na_{0.5}Bi_{0.5}TiO_3$-based systems. *Appl Phys Lett* 2016;108:202902. DOI
13. Liu Z, Ren P, Long C, Wang X, Wan Y, Zhao G. Enhanced energy storage properties of $NaNbO_3$ and $SrZrO_3$ modified $Bi_{0.5}Na_{0.5}TiO_3$ based ceramics. *J Alloy Compd* 2017;721:538-44. DOI
14. Zhang L, Pu Y, Chen M, et al. High energy-storage density under low electric fields and improved optical transparency in novel sodium bismuth titanate-based lead-free ceramics. *J Eur Ceram Soc* 2020;40:71-7. DOI
15. Wang C, Lou X, Xia T, Tian S. The dielectric, strain and energy storage density of BNT-BKH_xT_{1-x} piezoelectric ceramics. *Ceram Int* 2017;43:9253-8. DOI
16. Zhu X, Shi P, Kang R, et al. Enhanced energy storage density of $Sr_{0.7}Bi_xTiO_3$ lead-free relaxor ceramics via a-site defect and grain size tuning. *Chem Eng J* 2021;420:129808. DOI
17. Liu L, Fan H, Fang L, Chen X, Dammak H, Thi MP. Effects of Na/K evaporation on electrical properties and intrinsic defects in $Na_{0.5}K_{0.5}NbO_3$ ceramics. *Mater Chem Phys* 2009;117:138-41. DOI
18. Shi P, Zhu X, Lou X, et al. Tailoring ferroelectric polarization and relaxation of BNT-based lead-free relaxors for superior energy storage properties. *Chem Eng J* 2022;428:132612. DOI
19. Grace MAL, Sambasivam R, Perumal RN, Athikesavan V. Enhanced synthesis, structure, and ferroelectric properties of Nb-modified 1-*x*[$Bi_{0.5}(Na_{0.4}K_{0.1})(Ti_{1-x}Nb_x)$]$O_3$-*x*($Ba_{0.7}Sr_{0.3}$)$TiO_3$ ceramics for energy storage applications. *J Aust Ceram Soc* 2020;56:157-65. DOI
20. Viola G, Ning H, Wei X, et al. Dielectric relaxation, lattice dynamics and polarization mechanisms in $Bi_{0.5}Na_{0.5}TiO_3$-based lead-free ceramics. *J Appl Phys* 2013;114:014107. DOI
21. Shi P, Zhu X, Lou X, et al. $Bi_{0.5}Na_{0.5}TiO_3$-based lead-free ceramics with superior energy storage properties at high temperatures. *Compos Part B Eng* 2021;215:108815. DOI
22. Chen P, Chu B. Improvement of dielectric and energy storage properties in Bi($Mg_{1/2}Ti_{1/2}$)O_3-modified $(Na_{1/2}Bi_{1/2})_{0.92}Ba_{0.08}TiO_3$ ceramics. *J Eur Ceram Soc* 2016;36:81-8. DOI
23. Li W, Zhou D, Pang L. Enhanced energy storage density by inducing defect dipoles in lead free relaxor ferroelectric $BaTiO_3$-based ceramics. *Appl Phys Lett* 2017;110:132902. DOI
24. Zhao L, Liu Q, Gao J, Zhang S, Li JF. Lead-free antiferroelectric silver niobate tantalate with high energy storage performance. *Adv Mater* 2017;29:1701824. DOI
25. Wang T, Jin L, Li C, Hu Q, Wei X, Lupascu D. Relaxor ferroelectric $BaTiO_3$-Bi($Mg_{2/3}Nb_{1/3}$)O_3 ceramics for energy storage application. *J Am Ceram Soc* 2015;98:559-66. DOI
26. Shi P, Hong Z, Zhu X, et al. Enhancement of energy storage properties of $Bi_{0.5}Na_{0.5}TiO_3$-based relaxor ferroelectric under moderate electric field. *Appl Phys Lett* 2022;120:132903. DOI
27. Lou XJ. Polarization fatigue in ferroelectric thin films and related materials. *J Appl Phys* 2009;105:024101. DOI
28. Lou XJ, Zhang M, Redfern SAT, Scott JF. Fatigue as a local phase decomposition: a switching-induced charge-injection model. *Phys Rev B* 2007:75. DOI
29. Lou XJ, Zhang M, Redfern SA, Scott JF. Local phase decomposition as a cause of polarization fatigue in ferroelectric thin films. *Phys Rev Lett* 2006;97:177601. DOI PubMed